Supporting Information for

"Highly entangled photons from hybrid piezoelectric-semiconductor quantum dot devices"

by

Rinaldo Trotta[†,*], *Johannes S. Wildmann*[†], *Eugenio Zallo*[‡], *Oliver G. Schmidt*[‡], *and Armando Rastelli*[†]

[†] Institute of Semiconductors and Solid State Physics, Johannes Kepler University, Altenbergerstr.69, A-4040 Linz, Austria

[‡] Institute for Integrative Nanosciences, IFW Dresden, Helmholtzstr. 20, D-01069 Dresden, Germany.

Corresponding Author

Dr. Rinaldo Trotta

Institute of Semiconductor and Solid State Physics,

Johannes Kepler University Linz, Altenbergerstr. 69,

A-4040 Linz, Austria.

Tel.: +43 732 2468 9599

Fax: +43 732 2468 8650

e-mail: rinaldo.trotta@jku.at

Sample growth and device fabrication

In(Ga)As QDs were grown by molecular beam epitaxy. Following oxide desorption and buffer growth, a 100 nm thick $Al_{0.75}Ga_{0.25}As$ sacrificial layer was deposited before the following GaAs/$Al_{0.4}Ga_{0.6}$ layers: a 180 nm thick n-doped layer, a 150 nm thick intrinsic region containing the QDs, and a 100 nm thick p-doped layer. The QDs were grown at 500°C and capped by an indium flush technique. The sacrificial layer in combination with metal evaporation, optical lithography and wet-chemical etching were used to release 500 nm thick nanomembranes of rectangular shape (150x120 μm^2). Gold thermo-compression bonding was then used to transfer the nanomembranes onto 300 µm thick PMN-PT actuator and 25 µm aluminum wires were used to connect electrically the device to a chip carrier. Further details on the device fabrication and performances can be found elsewhere[1].

Micro-photoluminescence and photon-correlation spectroscopy

Conventional micro-photoluminescence spectroscopy was used for the optical characterization of the devices. The measurements were performed at low temperature (typically 4-10 K) in a helium flow cryostat. The QDs were excited non-resonantly at 850 nm with a femtosecond Ti:Sapphire laser having an 80 MHz repetition rate and focused by a microscope objective with 0.42 numerical aperture. The same objective was used for the collection of the photoluminescence signal, which was spectrally analyzed by single or double spectrometers featuring 0.75 m focal length per stage and equipped with 1200 or 1800 lines/mm gratings, and finally detected by a nitrogen-cooled silicon charge-coupled device. Polarization-resolved micro-photoluminescence experiments were performed combining a rotating half-wave plate and a linear polarizer placed before the entrance slit of the spectrometer. The transmission axis of the polarizer was set parallel to the [110] direction of the GaAs crystal (within 3°) and perpendicular to the entrance slit of the spectrometer, which defines the laboratory reference for vertical polarization. The FSS and the polarization angle of the excitonic emission were evaluated using the same procedure reported in reference 1, which ensures sub-microelectronvolt resolution.

For photon-correlation measurements, the signal was split into two parts after the microscope objective using a non-polarizing 50/50 beam splitter, spectrally filtered with two independent spectrometers tuned to the XX and X energies (the band-pass window of the spectrometers, ~ 100 μeV, is much larger than the typical linewidth of both transitions), and finally sent to two Hanbury Brown and Twiss setups (HBT) at the exits of the spectrometers. Each HBT consists of a polarizing 50/50 beam splitter placed in front of two avalanche photodiodes (APDs), whose output is connected to a 4-channel correlation electronics for reconstructing the second-order cross-correlation function between the XX and X photons. The temporal resolution of the system is about 400 ps, mainly limited by the time jitter of the APDs. In order to select the appropriate polarization basis for cross-correlation measurements, properly oriented half-wave plates and quarter-wave plates were placed right after the first non-polarizing beamsplitter. The experimental setup allows the second order cross-correlation function $g^{(2)}_{AB}$ in 4 different polarization settings (*AB*) to be evaluated with a single measurement, *i.e.*, $g^{(2)}_{AB}$, $g^{(2)}_{AA}$, $g^{(2)}_{BB}$, and $g^{(2)}_{BA}$ were measured simultaneously. This reduces considerably the time of the experiment and, consequently, the effect of possible sample drifts during correlation measurements.

Data analysis for correlation measurements

Raw data were used in the analysis reported in the main text, without any background light subtraction. The second order correlation function was evaluated using the following formula: $g^{(2)}_{AB} = R/(N/n)$, where R is the number of pairs detected in a 10 ns window (w) centered at zero time-delay, N is the number of pairs detected in the side-peaks and n is the number of side-peaks considered (20 in our case, each of them integrated over 10 ns). For a given polarization base AB, the degree of correlation was calculated as explained in the text and averaging the two possible polarization combinations, *i.e.* $C_{AB} = \frac{1}{2}\left(\frac{g^{(2)}_{AA} - g^{(2)}_{AB}}{g^{(2)}_{AA} + g^{(2)}_{AB}} + \frac{g^{(2)}_{BB} - g^{(2)}_{BA}}{g^{(2)}_{BB} + g^{(2)}_{BA}}\right)$. For the density matrix reconstruction we have used probabilities, calculated from the raw counts via the following formula: $P_{AB} = \frac{g^{(2)}_{AB}}{g^{(2)}_{AA} + g^{(2)}_{AB} + g^{(2)}_{BA} + g^{(2)}_{BB}}$. The errors for all the quantities used in the analysis, including fidelity and the three Bell's parameters listed in the main text, were propagated assuming a Poissonian distribution for R and N (and no error for n), *i.e.*, $\Delta R = \sqrt{R}$ and $\Delta N = \sqrt{N}$. It is worth mentioning that using raw counts (integrated counts of the zero-time delay peak) instead of probabilities leads to very similar results, with maximum concurrence of C=0.76±0.02.

Sources of entanglement degradation

In the main text we stated that the level of entanglement achieved with our source is not yet ideal and that temporal post-selection of the emitted photons can be employed to partially avoid some of the sources of entanglement degradation. In the following, we would like to discuss in more details this matter.

The degree of entanglement achieved in our work is mainly limited by two mechanisms: (*i*) depolarization of the intermediate X states caused by fluctuating QD environment and (*ii*) recapture processes. We expect background light originating from different regions of the sample as well as dark counts of our photon detectors to play a minor role (see the following). We discuss more in detail points (*i*) and (*ii*) below.

(*i*). *Fluctuating magnetic fields*. In the Figure 2 of the main text we show the degree of correlation in the linear, circular and diagonal base for a representative QD and we find $|C_{RL}|>C_{HV}\sim C_{DA}$. This is a common feature of the investigated QDs and usually observed in the literature. As explained in reference 2, this effect can be ascribed to the fluctuating magnetic fields produced by the QD nuclei that remove the degeneracy of the two bright excitonic states inducing sub-μeV fluctuations of the FSS.

Fluctuating electric fields. In most of the QDs investigated in our work we observe that the linewidth of the exciton transitions is ~40 μeV, a value which is not limited by the experimental spectral resolution. Furthermore, we often resolve spectral wandering of the QD emission lines. These effects can be ascribed to charges in the vicinity of the QD[3] that produce variation of the local electric field. Despite fluctuations in the lateral (in-plane) and vertical (along the QD growth direction) electric fields cannot explain the order of the degree of correlation in the different polarization basis, i.e., $|C_{RL}|>C_{HV}\sim C_{DA}$, we do expect they have an effect on their magnitude. Using the linewidth of the X line along with the known shift of its energy with the applied vertical electric field, we estimate a ~ 0.2 μeV fluctuation of the FSS if broadening would be only due to fluctuations of the electric field. Even larger effects are expected from lateral electric fields[4], though a quantitative estimation cannot be extracted from our experiment.

It is important to point out that these FSS fluctuations (produced by both electric and magnetic fields) are expected to occur on millisecond or microsecond timescales[2,5], *i.e.*, they are much faster than the time required for a polarization-resolved measurement (~ minutes) used to estimate the exciton FSS. As a result, we are able to measure s~0 μeV on average only. Since the intensity of the fluctuations may vary from QD to QD, this scenario also explains the small differences in the fidelity in all the parameters quantifying entanglement clearly visible in Figures 3 and 4 for the different QDs studied in this work.

(*ii*) An additional source of entanglement degradation is associated with processes in which the intermediate X level is re-excited to the XX level before it decays to the ground state. This mechanism, often referred to as recapture[6,7], can be optically driven or due to charged carriers trapped in the QD surrounding and produce background photons lowering the correlation visibilities. Specifically, it produces coincidence counts at negative time delays corresponding to events in which X photons are detected before XX photons. A close inspection of the bunching peak at zero time delay (see Figure S1a) reveals indeed a symmetric profile, which cannot be accounted for by the finite time response of our photon detectors only (~ 400 ps). Since in the analysis presented in the main text we integrate all the counts over a w=10 ns temporal window (see Figure S1a), recapture processes are limiting the degree of entanglement of our source.

Temporal post-selection of the emitted photons[6-8] can be used to alleviate the deleterious effects just discussed, and it is the subject of the following section. However, we would like to mention that the degree of entanglement can be further improved using different excitation schemes – such as quasi-resonant excitation[9,10]– and/or optimized sample design in which the QDs are sitting at larger distances from the doped regions of the diode. We leave these points for future studies.

Temporal post-selection of the emitted photons

In photon correlation measurements ($R_{XX}L_X$ for example, see Figure S1a), a clean XX-X cascade should appear as a strongly asymmetric bunching peak with an exponential tail for positive time delays. In our experiment, a series of effects lead to deviations from the expected behavior, finally resulting in almost symmetric bunching peaks (see Figure S1a). Firstly, the finite temporal resolution of the experimental set-up (~400 ps, comparable with the lifetime of the exciton transition ~1 ns) results in a pronounced broadening of the bunching peak, which therefore extends to negative time delays. Recapture processes also contribute to the number of counts recorded for negative time delays, as discussed in the previous section. Finally, in the presence of a fluctuating FSS, X photons arriving at longer time delays are expected to exhibit lower fidelity to the predicted Bell state ψ (see the main text). It is therefore quite clear that temporal post-selection or temporal gating of the emitted photons capable to filter photons pairs originating from "clean" XX-X cascades would increase the level of entanglement. Time-gating techniques have been successfully employed to exclude X photons arriving at longer time delays and a significant increase of the fidelity to the ψ state has been observed, also in the case of QDs with s substantially different from zero[6, 8]. Moreover, it has been shown recently that post-selection of the correlation counts used in the data analysis leads to very similar results[7]. Here, we adopt an approach similar to the latter and we study the evolution of all the parameters quantifying entanglement as a function of the temporal window *w* (see Figure S1a) we choose to integrate the correlation counts later used in the analysis. Differently from reference 7 and because of the limited temporal resolution of our photon detectors, we reduce the temporal window around the center of mass of the bunching peaks, i.e., we gradually and symmetrically discard photons arriving at longer positive and negative time delays.

Figure S1b shows the evolution of the tangle (T), entanglement of formation (E_F), concurrence (C), fidelity (*f*) and largest eigenvalue (λ) as a function of the fraction of coincidence counts (normalized to the total counts measured at w=10 ns) recorded during the binning procedure. The different points correspond to different *w*, ranging from 10 ns to 1 ns. A monotonic increase of all the parameters quantifying entanglement can be clearly observed. More specifically, we note a slight increase of the parameters for 4 ns$<w<$10 ns when less than 10% coincidence counts discarded. This behavior can be easily explained considering the temporal width of the bunching peak (~ 4 ns, see Figure S1a), and points out the small, albeit deleterious, effect of background photons. A more pronounced effect is instead observed for $w<$4 ns: When ~60% of the counts are discarded (w=1 ns) a concurrence as high as 0.82 is measured. This proves that temporal filtering can be used to partially avoid the effects of the sources of entanglement degradation discussed in the previous session and it also suggests that the use of faster photon detectors along with time-gating techniques[6,8] could be employed to increase even further the level of entanglement of our source. It is important to note that the measurements used for the analysis reported in Figure S1b are obtained at s~0 μeV, as confirmed by the absence of appreciable changes in the phase delay between $\left|H_{XX}H_X\right\rangle$ and $\left|V_{XX}V_X\right\rangle$, ϕ (see the inset of Figure S1b) with *w*. Furthermore, this also proves that this phase delay arises from artifacts of our collection optics, *i.e.*, from a reflection at our beam splitter (see the main text).

Finally, Figures S1c-d show the effect of the temporal filtering on the three Bell parameters listed in the main text and analyzed for two different values of the electric field F_d (and at a fixed F_p=17.3 kV/cm) where the minimum FSS occurs. In this region, fluctuations in the FSS lead to variations of the degree of correlation in the different polarization bases, thus causing fluctuations of the different Bell parameters. However, a general increase of S_{RD}, S_{RC}, and S_{CD} as a function of *w* can be clearly observed in both cases. If we consider the region around the minimum FSS, the maximum values of the three Bell parameters for *w*=2 ns (see Figure S1e) are S_{RD} =2.22 ± 0.05, S_{RC}=2.43 ± 0.04, and S_{CD}=2.50 ± 0.07, well above the Bell limit (for *w*=1 ns the reader is referred to the main text). Figures S1e-f show that the temporal filtering also extends the range of X energies where entangled photons are generated. In particular, the classical (Bell) limit can be violated when the X energy is tuned over 6 meV (1 meV). As discuss in the main text, this result is potentially interesting for interfacing distant QD-based entanglement resources, i.e., for entanglement swapping experiments with dissimilar QDs.

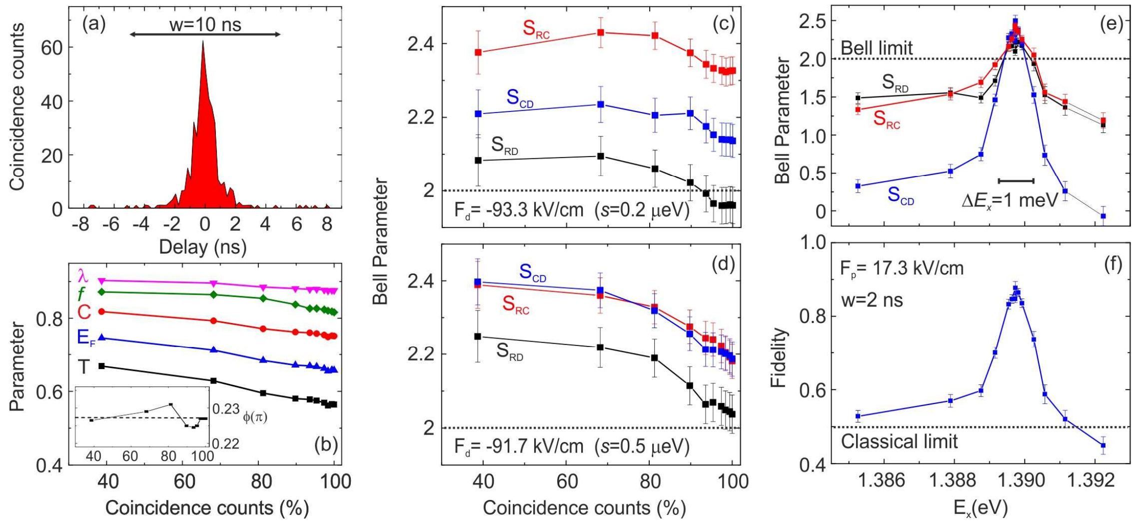

Figure S1. (a). Cross-correlation measurement in one of the investigated QDs for cross-circular XX-X photons and zoomed close to the zero-delay bunching peak. The solid line indicates the temporal window over which the correlation counts are integrated for the analysis presented in the main tex (*w*=10 ns). **(b)**. Evolution of the parameters quantifying entanglement (tangle T, entanglement of formation E_F, concurrence C, fidelity *f* to the expected Bell state and largest eigenvalue λ) as a function of the fraction of coincidence counts (normalized to the total counts measured at *w*=10 ns) recorded during the binning procedure. The inset shows the evolution of the phase delay between $\left|H_{XX}H_X\right\rangle$ and $\left|V_{XX}V_X\right\rangle$. The dashed line indicates the average value. **(c)**. Evolution of the three Bell parameters (see the main text) as a function of the fraction of coincidence counts recorded during the binning procedure and for F_d= -93.3 kV/cm and F_p= 17.3 kV/cm. The value of the FSS measured for these values of the electric fields is also indicated **(d)**. Same as (c) for F_d= -91.7 kV/cm and F_p= 17.3 kV/cm. The value of the FSS measured for these values of the electric fields is also indicated. **(e)**. The three Bell parameters as a function of the X energy for *w*=2 ns. The X energy is tuned via F_d while

F_p is kept fixed at F_p= 17.3 kV/cm. The dashed line indicates the Bell limit while the solid bar shows the range of X energies were non-local correlation between the emitted photons can be measured. **(f)**. Same as (e) for the fidelity to the expected Bell state f . The dashed line indicates the classical limit.

References

(1) Trotta, R.; Zallo, E.; Ortix, C.; Atkinson, P.; Plumhof, J. D.; Brink, J. V. D.; Rastelli, A.; Schmidt, O. G. *Phys. Rev. Lett.* **2012**, *109*, 147401.

(2) Stevenson, R. M.; Salter, C. L.; Boyer de la Giroday, A.; Farrer, I. A.; Nicoll, C. A.; Ritchie, D. A.; Shields, A. J. *ArXiv*:1103.2969.

(3) Houel, J.; Kuhlmann, A. V.; Greuter, L.; Xue, F.; Poggio, M.; Gerardot, B. D.; Dalgarno, P. A.; Badolato, A.; Petroff, P. M.; Ludwig, A.; Reuter, D.; Wieck, A. D.; Warburton, R. J. *Phys. Rev. Lett.* **2012**, *108*, 107401.

(4) Vogel, M. M.; Ulrich, S. M.; Hafenbrak, R.;, Michler, P.; Wang, L.; Rastelli, A.; Schmidt, O. G. *Appl. Phys. Lett.* **2007**, *91*, 051904.

(5) Prechtel, J. H.; Kuhlmann, A. V.; Houel, J.; Greuter, L.; Ludwig, A.; Reuter, D.; Wieck, A. D.; Warburton, R. J. *Phys. Rev. X* **2013**, *3*, 041006.

(6) Young, R. J.; Stevenson, R. M.; Hudson, A. J.; Nicoll, D. A.; Ritchie, D. A.; Shields, A. J. *Phys. Rev. Lett*. **2009**, *102*, 030406.

(7) Dousse, A.; Suffczyński, J.; Beveratos, A.; Krebs, O.; Lemaître, A.; Sagnes, I.; Bloch, J.; Voisin, P.; Senellart, P. *Nature* (London) **2010**, *466*, 217.

(8) Stevenson, R. M.; Hudson, A. J.; Bennett, A. J.; Young, R. J.; Nicoll, C. A.; Ritchie, D. A.; Shields, A. J. *Phys. Rev. Lett.* **2008**, *101*, 170501.

(9) Jayakumar, H.; Predojević, A.; Huber, T.; Kauten, T.; Solomon, G. S.; Weihs, G. *Phys. Rev. Lett*. **2013**, *110*, 135505.

(10) Müller, M.; Bounouar, S.; Jöns, K. D.; Glässl M.; Michler, P. *Nat. Photonics* **2014**, *8*, 224.